Hindawi
Advances in Civil Engineering
Volume 2021, Article ID 8839828, 9 pages
https://doi.org/10.1155/2021/8839828

Research Article

On Analysis of Seismic Vibrations Data Applying Doppler Effect Expression

J. Skeivalas, E. K. Paršeliūnas, D. Šlikas, R. Obuchovski, and R. Birvydienė

Institute of Geodesy, Vilnius Gediminas Technical University, Saulėtekis Av. 11, LT-10223 Vilnius, Lithuania

Correspondence should be addressed to D. Šlikas; dominykas.slikas@vgtu.lt

Received 28 September 2020; Revised 13 February 2021; Accepted 19 February 2021; Published 27 February 2021

Academic Editor: Claudio Mazzotti

In the paper, a possibility to develop the digital models of the seismic vibrations parameters is analyzed. To reach this goal, the observations at seismic station LUWI (Indonesia) were processed applying the statistical procedures. In fact, the biggest attention was given to the introduction of the Doppler effect expression and the employment of the theory of covariance functions. The trend in vectors of vibrations intensities values was detected and estimated upon using the least-squares method and polynomial approximation. In addition, by this technique, the random errors were eliminated partially. The self-developed computer programs based on Matlab programming package procedures were applied.

1. Introduction

Earthquake is one of the most costly, devastating, and deadly natural hazards. Every disaster damages thousands of buildings and displaces tens of thousands of people. The comprehensive knowledge of the earthquake nature and its behavior is extremely important. Here the main task for scientists is to constrain the suitable mathematical methods to analyse the earthquakes action, and most importantly to develop the earthquake model to predict its spread and to forecast its occurrence. The latest developments could be noted in [1–7], where the biggest efforts were taken for mathematical descriptions of wide earthquakes occurrence areas trying to construct the Ground Motion Prediction Equations. Deep analysis of different aspects of passive seismic methods like a horizontal to vertical spectral ratio, which is often used to describe the earthquake site, could be found in [8–14]. Some characteristics of concrete earthquake's sites from world's seismic zones are presented in [9, 15–22]. In some papers, the stress was done on significance of three-dimensional modelling of seismic waves propagation [18, 23–27].

Various data sources were applied to investigate the phenomena of eruptions [28–30]. Great achievements are done using modern techniques like InSAR interferometry [31–34], GNSS [35–38], and satellite imagery [39–42]. Several studies are dedicated to one of the most destructive eruptions—the 2018 Indonesia Sulawesi magnitude 7.5 Palu earthquake [34, 37, 41, 42].

For Indonesia, from which the practical example in this paper is given, some research results could be found in [43–50]. Indonesia has a high seismicity rate, which is related to complex interaction of several tectonic plates [51–63]. It should be especially noted that Indonesia's seismic region is an area of highest magnitude (more than 6.0) eruptions [37, 60, 64–70].

What deals with scientific techniques and methods to investigate earthquakes application has InSAR technology, which enables detecting surface slips and Earth surface deformations [34, 37, 41]. For example, the 4–7 m surface slip in the area of Palu earthquake was detected [37] and the maximum horizontal deformation was from 1.8 m till 3.6 m [41], when ALOS-2 interferogram showed a peak slip of 6.5 m located at the south of Palu city [34]. GNSS plays a great role in the research of earthquakes giving very precise metrical parameters to improve the crustal deformation field and 3D geometric complexities of the faults in total [38, 53, 60, 65, 68]. Certainly, the main techniques to detect the technical parameters of earthquakes are seismograms and the combinations of some techniques as well [34, 67]. So,

from broadband regional seismograms, it was revealed that the 2018 Palu earthquake is a supershear rupture event from early on with an average rupture velocity of 4.1 km/s, and the total seismic moment of 2.64×1020 Nm (equivalent to Mw 7.55) was released within 40 s [34].

In this paper, we will show how the Doppler effect expression and the application of the theory of covariance functions could be employed for seismic waves modelling. The practical calculations were executed using the two fragments of the observations data of the intensity φ of the Earth's seismic field, which were chosen from LUWI seismic station (Sulawesi, Indonesia, latitude: −1.04180, longitude: 122.77170, elevation: 6.0 m): first on August 05, 2018, within one hour (11:30–12:30), and second on November 11, 2018, within two hours (5:00–7:00). At these periods, the seismic stations around the world have registered unusual vibrations of low frequencies. Wide basic information on Palu earthquake could be found in specialized portals [71, 72].

The observations data were expressed by vectors N (North), E (East), and Z (Zenith). The time series views of the centered vectors N, E, and Z for both abovementioned periods are presented in Figures 1 and 2. In both figures, the time series views of the components E and N are similar. It looks like the influence of the unusual low frequencies vibrations in Figure 2 is possibly low. The systematic component of low frequency could be eliminated applying the 6-degree polynomial approximation. It is presented in Figure 3. The accuracy of vectors N, E, and Z extracted from LUWI station data on August 05, 2018, is described by standard deviations $S_\varphi = (19480, 15926, 15810)$ cnt. These numbers show that the accuracies of components of seismic vectors presented in Figure 1 are approximately the same. The accuracy of vectors N, E, and Z extracted from LUWI station on November 11, 2018 (if the systematic component is not eliminated), is described by the vector of standard deviations $S_\varphi = (1260, 559, 41)$ cnt. It shows that the accuracy of observations is slightly higher at this period. The accuracy of vectors N, E, and Z extracted on November 11, 2018 (if the systematic component is eliminated), is described by the vector of standard deviations $S_\varphi = (215, 257, 41)$ cnt. In this case, the obtained accuracy of processed observation data is considerably higher.

Mathematical-statistical methods are widely applied for data processing in geophysics, geodesy, and other Earth sciences [73–75]. To predict and develop the model of the spread of seismic vibrations, first of all, we assume that seismic waves from the quake hypocenter spread as harmonic vibrations of decreasing amplitudes in all the directions. So, we can assume also that the core structures of seismic observations at the tracking stations mounted in short distances from the hypocenter and at those more distant are possibly very similar. For mathematical treatment of the seismic observations, the covariance functions and the theory of Doppler effect were applied. The correlations between changes of intensities of seismic waves spreading in time and space were detected by introducing the variations of covariations of the seismic vibrations intensities vectors. Some equations were derived to obtain the estimates of covariation matrixes and autocovariances and cross-

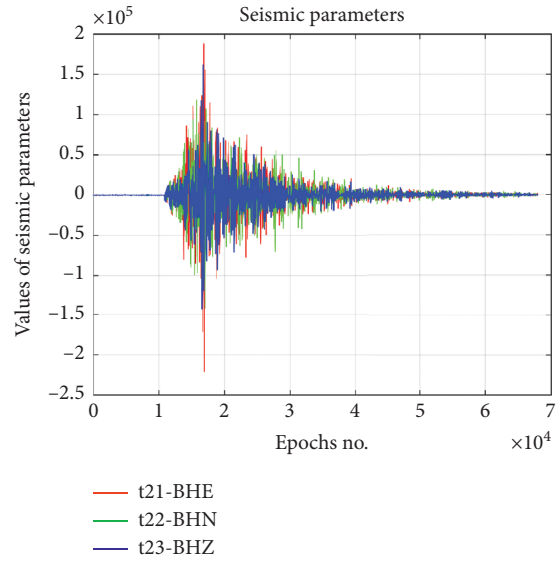

Figure 1: Time series of vectors N, E, and Z (LUWI station, August 05, 2018).

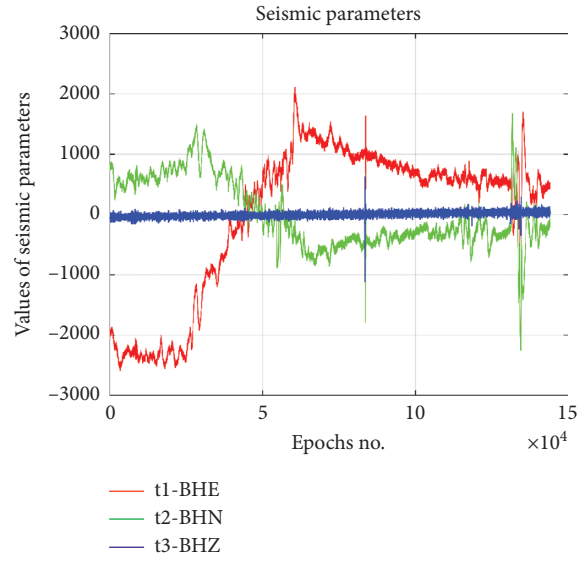

Figure 2: Time series of vectors N, E, and Z (LUWI station, November 11, 2018).

covariances of seismic field intensities vectors based on seismic observations data. The accuracies of corresponding calculated parameters were obtained also.

The background of the mathematical model of observations data treatment is concept of a stationary random function and especially paying attention to statement that the errors of seismic vibrations observations are random and possibly are near the same precision. So we assume that the mathematical average of random errors $M\Delta = \text{constant} \longrightarrow 0$, its dispersion $D\Delta = \text{constant}$, and the covariances of the observations depend on the difference of the arguments only, so practically from the quantised intervals on the time scale.

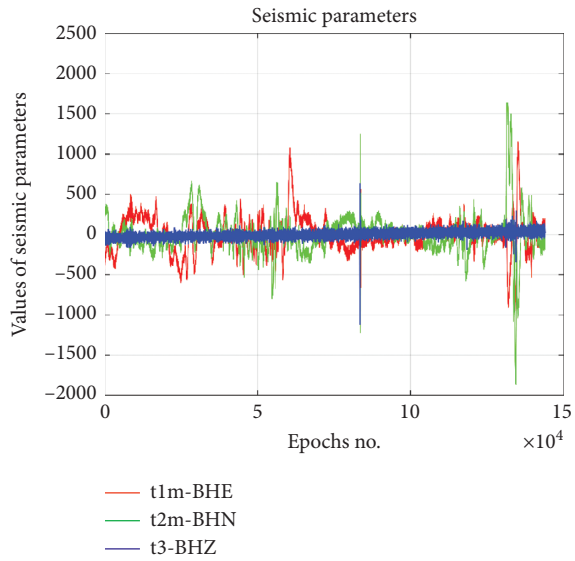

Figure 3: Time series of vectors N, E, and Z when the systematic component is eliminated (LUWI station, November 11, 2018).

2. Modelling of Seismic Vibrations

The observation data registered by the seismic station had been previously examined and processed upon reaching a goal to eliminate both random and possibly systematic errors.

The most reliable values of the trend in the seismic vibrations arrays were detected employing the least-squares method. Application of least-squares technique gives a possibility to eliminate the random errors partially. While treating the big volumes of observations, the least-squares technique produces the asymptotically efficient values of the derived parameters also in case when a statistical distribution of the observations errors is not normal.

Any vector of seismic vibrations intensities could be treated as a random function, which involves the random errors of observations. By employing a least-squares technique to treat the vector of intensities φ, we can detect the most reliable value $\widetilde{\varphi}$ of the trend. A parametric equation of a single vector's element φ_i will look like the following:

$$\varepsilon_i = \varphi_i - \widetilde{\varphi}, \tag{1}$$

where ε_i is a random error of the vector's element, φ_i is the value of the vector's element, and $\widetilde{\varphi}$ is vector's trend.

The expression in matrix form of equation (1) will be as follows:

$$\varepsilon = \varphi - e\widetilde{\varphi}, \tag{2}$$

where ε is vector of random errors, $\varphi = (\varphi_1, \varphi_2, \ldots, \varphi_n)^T$ is vector of seismic field intensities, and e is vector of units $(n \times 1)$.

The most reliable value of vector φ trend could be calculated by introducing the general condition of the least-square method:

$$\Phi = \varepsilon^T P \varepsilon = \min, \tag{3}$$

where P is diagonal matrix $(n \times n)$ of weights p_i of the values φ_i.

Weights p_i could be detected according to simple formula:

$$p_i = \frac{\sigma_0^2}{\sigma_{\varphi i}^2}, \tag{4}$$

where σ_0 is the standard deviation of the observation φ_0, the weight of which is supposed to be equal to unit, that is, $p_0 = 1$.

Furthermore, we can write the following equation:

$$u_i = \ln \varphi_i, \tag{5}$$

and we further obtain

$$\sigma_{\varphi i} = \sigma_{ui} \varphi_i. \tag{6}$$

From formula (6), we can see that the value of $\sigma_{\varphi i}$ pertains from the value of φ_i. So, the components, which have the bigger values, are of a lower accuracy just because $\varphi_i \gg \sigma_{ui}$.

Upon applying formula (4), we write

$$p_i = \frac{\sigma_0^2}{\sigma_{ui}^2 \varphi_i} = 5 \cdot \varphi_i^{-2} \cdot 10^4, \tag{7}$$

where the accepted average value is $\sigma_0^2/\sigma_{ui}^2 = 5 \cdot 10^4$.

To find the extremum of function (3), let us calculate its partial derivatives according to trend $\widetilde{\varphi}$. We can write and solve the equation:

$$\frac{\partial \Phi}{\partial \widetilde{\varphi}} = 2\left(\frac{\partial \varepsilon}{\partial \widetilde{\varphi}}\right)^T P \cdot \varepsilon = 0. \tag{8}$$

Then we will obtain

$$\begin{aligned} -e^T P \varepsilon &= 0, \\ e^T P e \widetilde{\varphi} - e^T P \varphi &= 0. \end{aligned} \tag{9}$$

Thus, we will get the following solution:

$$\widetilde{\varphi} = \left(e^T P e\right)^{-1} e^T P \varphi = N^{-1} \omega, \tag{10}$$

where $N = (e^T P e), \omega = e^T P \varphi$.

The accuracy of the trend could be detected by calculating its covariance matrix $K_{\widetilde{\varphi}}$:

$$K_{\widetilde{\varphi}}' = \sigma_{\widetilde{\varphi}}'^2 = \sigma_0'^2 N^{-1}, \tag{11}$$

where σ_0' is the estimate of the standard deviation σ_0. It is assessed by formula:

$$\sigma_0'^2 = \frac{1}{n-1} \varepsilon^T P \varepsilon, \tag{12}$$

The considerably high systematic component of the vibrations of the data of seismic station LUWI was eliminated upon applying a 6-degree polynomial approximation.

Now, it is possible to calculate cross-covariance and autocovariance functions of the seismic vibrations as well as

the shifts of the seismic vibrations, respectively, to each other by introducing the Doppler effect expression.

Let us take the formula for the parameter z [76–78]:

$$z = \frac{f_e}{f_o} - 1 = \frac{f_e - f_o}{f_o}, \tag{13}$$

where f_e is frequency of emitted vibrations and f_o is frequency of observed vibrations.

We accept that the changes of vibrations phases observed at tracking stations possibly correspond to the changes of the seismic vibrations intensities. Consequently, sum of the seismic vibrations intensities is proportional to the algebraic sum of the frequencies phases of vibrations accordingly; that is,

$$\delta B \sim \delta\omega; \tag{14}$$

here $\delta B, \delta\omega$ are changes of vibrations intensities and vibrations frequencies phases, respectively.

We can write the expressions for changes of vibrations intensities and the sum of them as follows:

$$\begin{aligned} \delta a(t) &= A\delta\omega \cdot \cos \omega t, \\ \delta a_e(t) - \delta a_o(t) &= A_e\delta\omega_e \cdot \cos \omega_e t - A_0\delta\omega_o \cdot \cos \omega_o t, \end{aligned} \tag{15}$$

where $\omega_e = 2\pi f_e, 2\pi f_o$, and the initial phases φ_0 are supposed to be equal to zero; $\delta a \longrightarrow \delta B$.

By employing the parameter z of the Doppler effect formula, we can express the strength of the seismic vibrations at the moment in time t_i:

$$z_i \cong \frac{\delta B_{\mathrm{ei}}}{\delta B_{\mathrm{oi}}} - 1 = \frac{\delta B_{\mathrm{ei}} - \delta B_{\mathrm{oi}}}{\delta B_{\mathrm{oi}}}, \tag{16}$$

where B_{ei} is the intensity of emitted seismic vibrations, B_{oi} is the intensity of observed seismic vibrations, $B_{\mathrm{ei}} \sim \omega_{\mathrm{ei}}$, and $B_{\mathrm{oi}} \sim \omega_{\mathrm{oi}}$.

In further developments, we employ the theory of covariance functions to detect the value of the argument z from the Doppler effect expression. Mathematical derivations are grounded on the conception of a stationary random function considering that errors of observations of seismic vibrations are random and possibly have similar precision.

It is possible to express a cross-covariance function of the straight algebraic sum $\Delta B_{\mathrm{ei}} = B_{\mathrm{ei}} - B_{\mathrm{oi}}$ of the two intensities B_{ei} and B_{oi} (emitted and observed) at a moment in time t_i and a separate intensity B_{oi} as follows:

$$\begin{aligned} K(\Delta B_{\mathrm{ei}}) &= K(\delta\Delta B_{\mathrm{ei}}) = M(\delta\Delta B_{\mathrm{ei}} \cdot \delta B_{\mathrm{oi}}) \\ &= M\{[\delta B_{\mathrm{oi}}(z_i + 1) - \delta B_{\mathrm{oi}}] \cdot \delta B_{\mathrm{oi}}\} \\ &= M(\delta^2 B_{\mathrm{oi}}) \cdot Mz_i = \sigma_B^2 . Mz_i, \end{aligned} \tag{17}$$

where $\delta B_{\mathrm{oi}} = B_{\mathrm{oi}} - MB_{\mathrm{oi}}, \delta B_{\mathrm{ei}} = B_{\mathrm{ei}} - MB_{\mathrm{ei}}, \delta B_{\mathrm{ei}} = \delta B_{\mathrm{oi}}(z_i + 1), MB_{\mathrm{oi}}, MB_{\mathrm{ei}}$ are the average values of vibrations intensities; $\delta\Delta B_{\mathrm{oi}} = \delta B_{\mathrm{ei}} - \delta B_{\mathrm{oi}}, \sigma_B$ are the standard deviations of the vibrations intensities. It is supposed that the standard deviations of the observed and registered seismic vibrations intensities are equal.

The average magnitude M_{zi} of an argument z of the Doppler formula could be expressed upon introducing the vibrations intensities at the moment in time t_i applying the following formula:

$$M_{zi} = \frac{1}{\sigma_B^2} K(\Delta B_{\mathrm{ei}}, B_{\mathrm{oi}}). \tag{18}$$

By employing the theory of the covariance functions, it is possible to express the cross-covariance functions of the corresponding seismic vibrations vectors taking into account the fact that every vector of vibrations intensities could be treated as a random function as follows [77, 79, 80]:

$$\begin{aligned} K(\Delta B_e, B_o) &= K_z(\tau) = M\{\delta\Delta B_e(u) \cdot \delta B_o(u + \tau)\}, \\ \text{or } K_z(\tau) &= \frac{1}{T - \tau} \int_0^{T-\tau} \delta\Delta B_e(u) \cdot \delta B_o(u + \tau)\mathrm{d}u, \end{aligned} \tag{19}$$

where u is argument of any seismic vibrations vector, $\tau = s \cdot \Delta$ is quantised interval, which is variable, s is number of quantised intervals, Δ is the value of the accepted unit of observations, and T is the diapason of the fluctuations of seismic vectors elements.

By using the vectors of observations data, an estimation $K_z'(\tau)$ of the cross-covariance function could be calculated according to the following formula:

$$K_z'(\tau) = K_z'(s) = \frac{1}{n - s} \sum_{i=1}^{n-s} \delta\Delta B_e(u_i) \cdot \delta B_o(u_{i+s}), \tag{20}$$

where n is number of vector elements.

Now, using formula (18) in the vector form, we get the formula to detect the mathematical average of the argument z of the Doppler effect expression:

$$Mz = \frac{K_z'(s)}{m.\sigma_B'^2} = \frac{K_z'(s)}{m.K_z'(0)}, \tag{21}$$

where $\sigma_B'^2 \longrightarrow K_z'(0)$ is the estimate of the dispersion and m is number of cross-covariance values.

3. Analysis of the Experimental Results

The estimates of autocovariance and cross-covariance functions of the seismic vibrations intensities could be calculated employing formula (20). The values of the quantised intervals were assigned from 1 to $n/2$. Here, $n = 144000$ is the number of seismic vibrations vector components. The graphical images of autocovariance and cross-covariance functions were generated also. Some graphical images of covariance functions are shown in Figures 4–9.

Upon applying formula (21), the mathematical averages of the argument z of the Doppler expression were detected. The positive values of the argument z point out that the seismic vibrations recede from each other. The negative values of the argument z indicate that seismic vibrations approach each other. The calculated approximate reciprocal velocity of seismic vibrations, registered in vectors N and E, is about $v = 90$ km/s.

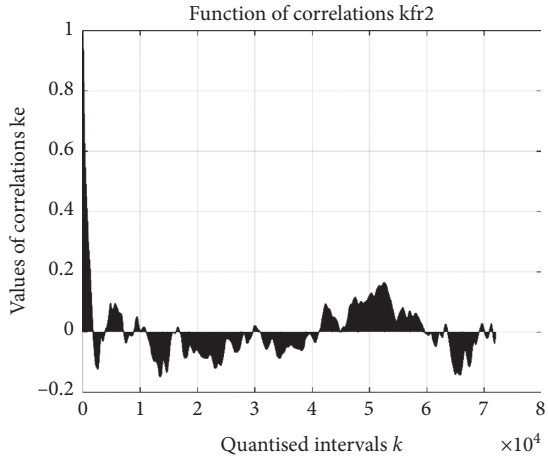

Figure 4: Image of the normed autocovariance function of the vector N.

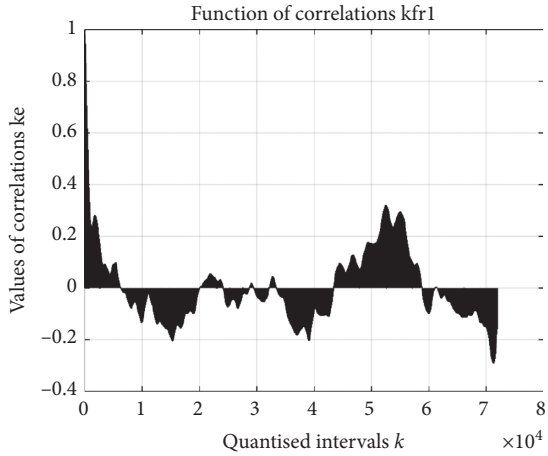

Figure 5: Image of the normed autocovariance function of the vector E.

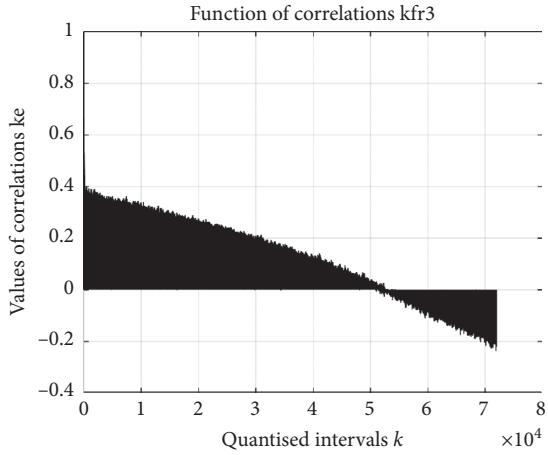

Figure 6: Image of the normed autocovariance function of the vector Z.

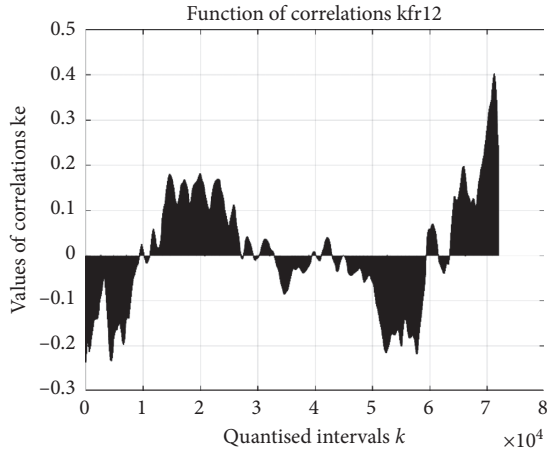

Figure 7: Image of the normed cross-covariance function of the two vectors N and E.

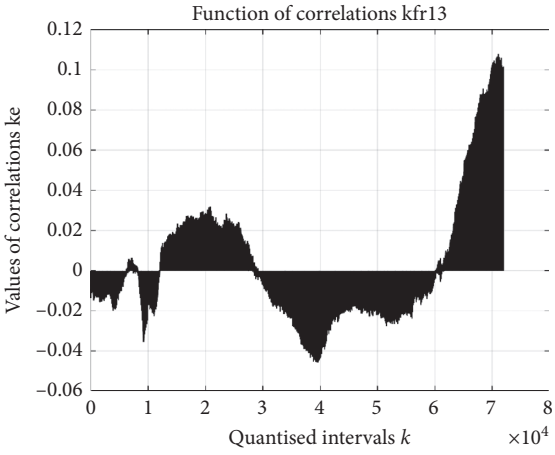

Figure 8: Image of the normed cross-covariance function of the two vectors E and Z.

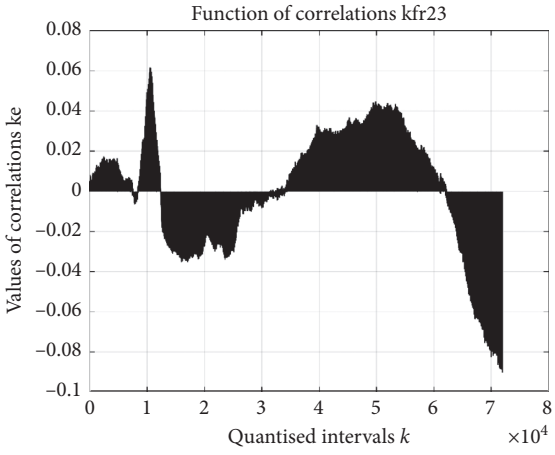

Figure 9: Image of the normed cross-covariance function of the two vectors N and Z.

Let us derive the estimates of the standard deviation of the argument z. It could be done in two ways. Firstly, z values could be detected upon applying the frequencies of vibrations emitted from earthquake source and observed frequencies of vibrations at seismic station. Secondly, z values could be detected using the vibrations intensities.

The formula to calculate the estimate of standard deviation of the argument z using formula (13) could be written as follows:

$$\sigma_z^2 = \frac{1}{f_o^2}\sigma_{fe}^2 + \frac{f_e^2}{f_o^4}\sigma_{fo}^2 = \frac{\sigma_{fo}^2}{f_o^2}\left(\frac{\sigma_{fe}^2}{\sigma_{fo}^2} + \frac{f_e^2}{f_o^2}\right) = 2\cdot 10^{-16}\left\{1 + (z+1)^2\right\} = 10\cdot 10^{-16}, \tag{22}$$

$$\sigma_z' = 3.0\cdot 10^{-8}. \tag{23}$$

In formula (22), the estimate σ_z' of the standard deviation of the argument z was detected assuming $\sigma_{fe} = \sigma_{fo}$, $z = 1.0$, and $\sigma_{fe}/\sigma_{fo} = 1.4\cdot 10^{-8}$. So, the ratio of the mathematical average of the argument z is $\sigma_z'/z = 3.0\cdot 10^{-8}$.

Let us derive the accuracy of the argument z of the Doppler effect expression using the seismic vibrations intensities. Upon applying formulas (15), (16), and (22), we have

$$\sigma_{z_B}^2 = \frac{\sigma_{B_o}^2}{B_o^2}\left\{1 + (z+1)^2\right\} = \frac{\sigma_{\omega_o}^2}{\omega_o^2}\cdot\left\{1 + (z+1)^2\right\},$$
$$\sigma_{z_B} = 2.2\,\frac{\sigma_{\omega_o}}{\omega_o} = 2.2\cdot 1.4\cdot 10^{-8} = 3\cdot 10^{-8}, \tag{24}$$

and the above was calculated upon considering $\sigma_{B_q} = \sigma_{B_o}$, $\sigma_{f_o}/f_o = \sigma_{\omega_o}/\omega_o$, and $z = 1.0$. The ratio of z_B will be $\sigma_{z_B}/z_B = 3\cdot 10^{-8}$.

The results of the calculations demonstrate that the detected accuracies of the argument z of the Doppler effect expression are nearly the same in both cases: when registered phases of vibrations frequencies or intensities (strengths) of them are used in the calculation procedures.

Let us calculate the accuracy of the estimates of the motion speed $v = z\cdot c$. Upon using the equation

$$\ln v = \ln z + \ln c, \tag{25}$$

we can write the equation of the ratio as follows:

$$\frac{\sigma_v^2}{v^2} = \frac{\sigma_z^2}{z^2} + \frac{\sigma_c^2}{c^2}, \tag{26}$$

and $(\sigma_v/v) \approx 3.0\cdot 10^{-9}$, when $(\sigma_c/c) = 3.0\cdot 10^{-9}$.

Introducing the above used data, we find that $(\sigma_v/v) = 3.0\cdot 10^{-6}$ km/s, upon supposing that $v = 1000$ km/s.

4. Conclusions

(1) It was shown that employment of the Doppler effect expression and the application of the theory of covariance functions could be used to develop the digital models of the seismic vibrations. A method was suggested to detect the values of argument z from the Doppler effect formulas upon employing the expression of the cross-covariance function of the sum of the intensities of seismic vectors components and the intensities of separate seismic vector components.

(2) For LUWI seismic station, the expressions of the normed autocovariance functions of seismic vibrations vectors N, E, and Z are slightly different. The autocovariance of the components of seismic vector Z has a maximum value of correlation $r = 0.4$. The autocovariance of seismic vibrations vectors components is deep $r \longrightarrow 1.0$ at little values of quantised interval only, when $k \longrightarrow 0$ ($\tau_k \longrightarrow 0$ s). The probabilistic dependence of the vector's Z elements gradually decreases to $r \longrightarrow 0$ at $k \longrightarrow 50000$ ($\tau_k \longrightarrow 2500$ s). The autocovariance functions of the vectors N and E have the low variable positive and negative values.

(3) The correlation values r of the normed cross-covariance functions of components of vectors N, E, and Z of tracking station are varying in a narrow range $r \longrightarrow (-0.2: 0.4)$ along the whole quantised diapason. The values r of normed cross-covariance functions of components of vectors N, E, and Z are close to zero.

(4) The speed of reciprocal motion of seismic vector E and N components was calculated. Its approximate value $v = 90$ km/s.

Data Availability

All data used during the research are available in a repository online in accordance with funder data retention policies. Practically, data for this research were taken from the EIDA and GEOFON Data Archives (http://eida.gfz-potsdam.de/webdc3/).

Disclosure

The research was done as a part of employment at Vilnius Gediminas Technical University, Lithuania.

Conflicts of Interest

The authors declare that there are no conflicts of interest.

References

[1] B.-J. Chiou and R. R. Youngs, "An NGA model for the average horizontal component of peak ground motion and response spectra," *Earthquake Spectra*, vol. 24, no. 1, pp. 173–215, 2008.

[2] B. S.-J. Chiou and R. R. Youngs, "Update of the chiou and youngs NGA model for the average horizontal component of peak ground motion and response spectra," *Earthquake Spectra*, vol. 30, no. 3, pp. 1117–1153, 2014.

[3] K. W. Campbell and Y. Bozorgnia, "NGA-West2 ground motion model for the average horizontal components of PGA, PGV, and 5% damped linear acceleration response spectra," *Earthquake Spectra*, vol. 30, no. 3, pp. 1087–1115, 2014.

[4] M. A. Marafi, M. O. Eberhard, and J. W. Berman, "Effects of the yufutsu basin on structural response during subduction earthquakes," in *Proceedings of the Sixteenth World Conference on Earthquake Engineering*, Santiago, Chili, January 2017.

[5] N. A. Abrahamson, W. J. Silva, and R. Kamai, "Summary of the ASK14 ground motion relation for active crustal regions," *Earthquake Spectra*, vol. 30, no. 3, pp. 1025–1055, 2014.

[6] N. Abrahamson, N. Gregor, and K. Addo, "BC hydro ground motion prediction equations for subduction earthquakes," *Earthquake Spectra*, vol. 32, no. 1, pp. 23–44, 2016.

[7] B. Pandey, R. S. Jakka, A. Kumar, and H. Mittal, "Site characterization of strong-motion recording stations of Delhi using joint inversion of phase velocity dispersion and H/V curve," *Bulletin of the Seismological Society of America*, vol. 106, no. 3, pp. 1254–1266, 2016.

[8] G. Tarabusi and R. Caputo, "The use of HVSR measurements for investigating buried tectonic structures: the Mirandola anticline, Northern Italy, as a case study," *International Journal of Earth Sciences*, vol. 106, no. 1, pp. 341–353, 2016.

[9] J. F. Borges, H. G. Silva, R. J. G. Torres et al., "Inversion of ambient seismic noise HVSR to evaluate velocity and structural models of the Lower Tagus Basin, Portugal," *Journal of Seismology*, vol. 20, no. 3, pp. 875–887, 2016.

[10] U. N. Prabowo, Marjiyono, and Sismanto, "Mapping the fissure potential zones based on microtremor measurement in Denpasar City, Bali," *IOP Conference Series: Earth and Environmental Science*, vol. 29, Article ID 012012, 2016.

[11] E. Fergany and K. Omar, "Liquefaction potential of Nile delta, Egypt," *NRIAG Journal of Astronomy and Geophysics*, vol. 6, no. 1, pp. 60–67, 2017.

[12] A. P. Singh, A. Shukla, M. R. Kumar, and M. G. Thakkar, "Characterizing surface geology, liquefaction potential, and maximum intensity in the kachchh seismic zone, western India through microtremor analysis," *Bulletin of the Seismological Society of America*, vol. 107, no. 3, 2017.

[13] V. Pazzi, L. Tanteri, G. Bicocchi, M. D'Ambrosio, A. Caselli, and R. Fanti, "H/V measurements as an effective tool for the reliable detection of landslide slip surfaces: case studies of Castagnola (La Spezia, Italy) and Roccalbegna (Grosseto, Italy)," *Physics and Chemistry of the Earth, Parts A/B/C*, vol. 98, pp. 136–153, 2017.

[14] N. A. Zeid, E. Corradini, S. Bignardi, V. Nizzo, and G. Santarato, "The passive seismic technique "HVSR" as a reconnaissance tool for mapping paleo-soils: the case of the pilastri archaeological site, northern Italy," *Archaeological Prospection*, vol. 24, no. 3, pp. 245–258, 2017.

[15] M. V. Manakou, D. G. Raptakis, F. J. Chávez-García, P. I. Apostolidis, and K. D. Pitilakis, "3D soil structure of the Mygdonian basin for site response analysis," *Soil Dynamics and Earthquake Engineering*, vol. 30, no. 11, pp. 1198–1211, 2010.

[16] M. Pilz, S. Parolai, M. Stupazzini, R. Paolucci, and J. Zschau, "Modelling basin effects on earthquake ground motion in the Santiago de Chile basin by a spectral element code," *Geophysical Journal International*, vol. 187, no. 2, pp. 929–945, 2011.

[17] A. Iwaki and T. Iwata, "Estimation of three-dimensional boundary shape of the Osaka sedimentary basin by waveform inversion," *Geophysical Journal International*, vol. 186, no. 3, pp. 1255–1278, 2011.

[18] V. M. Cruz-Atienza, J. Tago, J. D. Sanabria-Gomez et al., "Long duration of ground motion in the paradigmatic valley of Mexico," *Nature*, vol. 6, no. 38807, 2016.

[19] A. Berbellini, A. Morelli, and A. M. G. Ferreira, "Ellipticity of Rayleigh waves in basin and hard-rock sites in Northern Italy," *Geophysical Journal International*, vol. 11, no. 2, pp. 115–129, 2016.

[20] A. Berbellini, A. Morelli, and A. M. G. Ferreira, "Crustal structure of northern Italy from the ellipticity of Rayleigh waves," *Physics of the Earth and Planetary Interiors*, vol. 265, pp. 1–14, 2017.

[21] V. C. Tsai, D. C. Bowden, and H. Kanamori, "Explaining extreme ground motion in Osaka basin during the 2011 Tohoku earthquake," *Geophysical Research Letters*, vol. 44, no. 14, pp. 7239–7244, 2017.

[22] K. Chimoto, H. Yamanaka, S. Tsuno, H. Miyake, and N. Yamada, "Estimation of shallow S-wave velocity structure using microtremor array exploration at temporary strong motion observation stations for aftershocks of the 2016 Kumamoto earthquake," *Earth, Planets and Space*, vol. 68, no. 1, p. 206, 2016.

[23] S. Castellaro, L. A. Padrón, and F. Mulargia, "The different response of apparently identical structures: a far-field lesson from the Mirandola 20th May 2012 earthquake," *Bulletin of Earthquake Engineering*, vol. 12, no. 5, pp. 2481–2493, 2014.

[24] M. A. Denolle, E. M. Dunham, G. A. Prieto, and G. C. Beroza, "Strong ground motion prediction using virtual earthquakes," *Science*, vol. 343, no. 6169, pp. 399–403, 2014.

[25] L. Viens, H. Miyake, and K. Koketsu, "Long-period ground motion simulation of a subduction earthquake using the offshore-onshore ambient seismic field," *Geophysical Research Letters*, vol. 42, no. 13, pp. 5282–5289, 2015.

[26] L. Viens, H. Miyake, and K. Koketsu, "Simulations of long-period ground motions from a large earthquake using finite rupture modeling and the ambient seismic field," *Journal of Geophysical Research: Solid Earth*, vol. 121, no. 12, pp. 8774–8791, 2016.

[27] L. Viens, M. Denolle, H. Miyake, S. I. Sakai, and S. Nakagawa, "Retrieving impulse response function amplitudes from the ambient seismic field," *Geophysical Journal International*, vol. 210, no. 1, pp. 210–222, 2017.

[28] F. Løvholt, H. Hasan, S. Lorito et al., "Multiple source sensitivity study to model the 28 September Sulawesi tsunami—landslide and strike slip sources," in *Proceedings of the AGU Fall Meeting 2018*, Washington, DC, USA, December 2018.

[29] A. Van Dongeren, D. Vatvani, and M. van Ormondt, "Simulation of 2018 tsunami along the coastal areas in the Palu bay," in *Proceedings of the AGU Fall Meeting 2018*, Washington, DC, USA, December 2018.

[30] R. Omira, G. G. Dogan, R. Hidayat et al., "The September 28th, 2018, tsunami in Palu-Sulawesi, Indonesia: a post-event field survey," *Pure and Applied Geophysics*, vol. 176, no. 4, pp. 1379–1395, 2019.

[31] A. Hooper, D. Bekaert, K. Spaans, and M. Arıkan, "Recent advances in SAR interferometry time series analysis for measuring crustal deformation," *Tectonophysics*, vol. 514–517, pp. 1–13, 2012.

[32] M. Lesko, J. Papco, M. Bakon, and P. Liscak, "Monitoring of natural hazards in Slovakia by using of satellite radar interferometry," *Procedia Computer Science*, vol. 138, pp. 374–381, 2018.

[33] A. M. Lubis, T. Sato, N. Tomiyama, N. Isezaki, and T. Yamanokuchi, "Ground subsidence in Semarang-Indonesia investigated by ALOS-PALSAR satellite SAR interferometry," *Journal of Asian Earth Sciences*, vol. 40, no. 5, pp. 1079–1088, 2011.

[34] J. Fang, C. Xu, Y. Wen et al., "The 2018 Mw 7.5 Palu earthquake: a supershear rupture event constrained by InSAR and broadband regional seismograms," *Remote Sensing*, vol. 11, no. 11, p. 1330, 2019.

[35] A. Walpersdorf, C. Rangin, and C. Vigny, "GPS compared to long-term geologic motion of the north arm of Sulawesi," *Earth and Planetary Science Letters*, vol. 159, no. 1-2, pp. 47–55, 1998a.

[36] A. Walpersdorf, C. Vigny, C. Subarya, and P. Manurung, "Monitoring of the Palu-Koro fault (Sulawesi) by GPS," *Geophysical Research Letters*, vol. 25, no. 13, pp. 2313–2316, 1998b.

[37] A. Socquet, J. Hollingsworth, E. Pathier, and M. Bouchon, "Evidence of supershear during the 2018 magnitude 7.5 Palu earthquake from space geodesy," *Nature Geoscience*, vol. 12, no. 3, pp. 192–199, 2019.

[38] T. Tabei, F. Kimata, T. Ito et al., "Geodetic and geomorphic evaluations of earthquake generation potential of the Northern Sumatran Fault, Indonesia," in *Proceedings of the International Association of Geodesy Symposia, International Symposium on Geodesy for Earthquake and Natural Hazards (GENAH)*, Kyoto, Japan, June 2015.

[39] M. De Michele, "Subpixel offsets of copernicus sentinel 2 data, related to the displacement field of the Sulawesi earthquake (2018, M_w 7.5)," 2019.

[40] S. Valkaniotis, A. Ganas, V. Tsironi, and A. Barberopoulou, "A preliminary report on the M7.5 Palu 2018 earthquake co-seismic ruptures and landslides using image correlation techniques on optical satellite data," 2018.

[41] Y. Wang, W. Feng, K. Chen, and S. Samsonov, "Source characteristics of the 28 september 2018 M_w 7.4 Palu, Indonesia, earthquake derived from the advanced land observation satellite 2 data," *Remote Sensing*, vol. 11, no. 17, p. 1999, 2019.

[42] M. Syifa, P. Kadavi, and C.-W. Lee, "An artificial intelligence application for post-earthquake damage mapping in palu, central Sulawesi, Indonesia," *Sensors*, vol. 19, no. 3, p. 542, 2019.

[43] E. Saygin, P. R. Cummins, A. Cipta et al., "Imaging architecture of the Jakarta Basin, Indonesia with transdimensional inversion of seismic noise," *Geophysical Journal International*, vol. 204, no. 2, pp. 918–931, 2016.

[44] E. Saygin, P. R. Cummins, and D. Lumley, "Retrieval of the *P* wave reflectivity response from autocorrelation of seismic noise: Jakarta Basin, Indonesia," *Geophysical Research Letters*, vol. 44, no. 2, pp. 792–799, 2017.

[45] M. Ridwan, S. Widiyantoro, M. Irsyam, Afnimar, and H. Yamanaka, "Development of engineering bedrock map beneath Jakarta based on microtremor array measurements," *Geological Society, London, Special Publications*, vol. 441, no. 1, pp. 153–165, 2016.

[46] A. Cipta, R. Robiana, J. Griffin, N. Horspool, S. Hidayati, and P. Cummins, "A probabilistic seismic hazard assessment for Sulawesi, Indonesia," in *Geohazards in Indonesia: Earth Science for Disaster Risk Reduction Geol. Soc., London, Special Publications 441*, P. R. Cummins and I. Meilano, Eds., The Geological Society of London, London, UK, 2016.

[47] A. Cipta, P. Cummins, M. Irsyam, and S. Hidayati, "Basin resonance and seismic hazard in jakarta, Indonesia," *Geosciences*, vol. 8, no. 4, p. 128, 2018.

[48] L. Handayani, M. Maryati, K. Kamtono, M. Mukti, and Y. Sudrajat, "Audio-magnetotelluric modeling of cimandiri fault zone at Cibeber, Cianjur," *Indonesian Journal on Geoscience*, vol. 4, pp. 39–47, 2017.

[49] A. Koulali, S. McClusky, S. Susilo et al., "The kinematics of crustal deformation in Java from GPS observations: implications for fault slip partitioning," *Earth and Planetary Science Letters*, vol. 458, pp. 69–79, 2017.

[50] A. M. Pramatadie, H. Yamanaka, K. Chimoto et al., "Microtremor exploration for shallow S-wave velocity structure in Bandung basin, Indonesia," *Exploration Geophysics*, vol. 48, no. 4, pp. 401–412, 2016.

[51] J. A. Katili, "Large transcurrent faults in Southeast Asia with special reference to Indonesia," *Geologische Rundschau*, vol. 59, no. 2, pp. 581–600, 1970.

[52] N. Hurukawa, B. R. Wulandari, and M. Kasahara, "Earthquake history of the Sumatran fault, Indonesia, since 1892, derived from relocation of large earthquakes," *Bulletin of the Seismological Society of America*, vol. 104, no. 4, pp. 1750–1762, 2014.

[53] A. Julzarika and C. A. Rokhmana, "Detection of vertical deformation in Jakarta-Bandung high speed train route using X sar and sentinel," *Geodesy and Cartography*, vol. 45, no. 4, pp. 169–176, 2019.

[54] D. H. Natawidjaja, "Updating active fault maps and sliprates along the Sumatran Fault Zone, Indonesia," *IOP Conference Series: Earth and Environmental Science*, vol. 118, no. 1, Article ID 012001, 2018.

[55] O. Bellier, M. Sébrier, T. Beaudouin et al., "High slip rate for a low seismicity along the Palu-Koro active fault in central Sulawesi (Indonesia)," *Terra Nova*, vol. 13, no. 6, pp. 463–470, 2001.

[56] O. Bellier, M. Sébrier, D. Seward, T. Beaudouin, M. Villeneuve, and E. Putranto, "Fission track and fault kinematics analyses for new insight into the Late Cenozoic tectonic regime changes in West-Central Sulawesi (Indonesia)," *Tectonophysics*, vol. 413, no. 3-4, pp. 201–220, 2006.

[57] M. R. Daryono, "Paleoseismologi tropis Indonesia (dengan studi kasus di sesar sumatra, sesar palukoro-matano, dan sesar lembang)," 2018.

[58] O. Heidbach, M. Rajabi, X. Cui et al., "The World stress map database release 2016: crustal stress pattern across scales," *Tectonophysics*, vol. 744, pp. 484–498, 2018.

[59] E. Pelinovsky, D. Yuliadi, G. Prasetya, and R. Hidayat, "The 1996 Sulawesi tsunami," *Natural Hazards*, vol. 16, no. 1, pp. 29–38, 1997.

[60] A. Socquet, W. Simons, C. Vigny et al., "Microblock rotations and fault coupling in SE Asia triple junction (Sulawesi, Indonesia) from GPS and earthquake slip vector data," *Journal of Geophysical Research*, vol. 111, no. B8, Article ID B08409, 2006.

[61] Y. Tanioka, Yudhicara, T. Kususose et al., "Rupture process of the 2004 great Sumatra-Andaman earthquake estimated from tsunami waveforms," *Earth, Planets and Space*, vol. 58, no. 2, pp. 203–209, 2006.

[62] A. Cipta, R. Robiana, J. D. Griffin, N. Horspool, S. Hidayati, and P. R. Cummins, "A probabilistic seismic hazard assessment for Sulawesi, Indonesia," *Geological Society, London, Special Publications*, vol. 441, no. 1, pp. 133–152, 2017.

[63] I. M. Watkinson and R. Hall, "Fault systems of the eastern Indonesian triple junction: evaluation of Quaternary activity and implications for seismic hazards," *Geological Society, London, Special Publications*, vol. 441, no. 1, pp. 71–120, 2017.

[64] R. Zuo, C. Qu, X. Shan, G. Zhang, and X. Song, "Coseismic deformation fields and a fault slip model for the M_w7.8 mainshock and M_w7.3 aftershock of the Gorkha-Nepal 2015 earthquake derived from Sentinel-1A SAR interferometry," *Tectonophysics*, vol. 686, pp. 158–169, 2016.

[65] X. Song, Y. Zhang, X. Shan, Y. Liu, W. Gong, and C. Qu, "Geodetic observations of the 2018 M_w 7.5 Sulawesi earthquake and its implications for the kinematics of the Palu fault," *Geophysical Research Letters*, vol. 46, no. 8, pp. 4212–4220, 2019.

[66] H. Bao, J.-P. Ampuero, L. Meng et al., "Early and persistent supershear rupture of the 2018 magnitude 7.5 Palu earthquake," *Nature Geoscience*, vol. 12, no. 3, pp. 200–205, 2019.

[67] Y. Zhang, Y.-T. Chen, and W. Feng, "Complex multiple-segment ruptures of the 28 September 2018, Sulawesi, Indonesia, earthquake," *Science Bulletin*, vol. 64, no. 10, pp. 650–652, 2019.

[68] T. Ulrich, S. Vater, E. H. Madden et al., "Coupled, physics-based modeling reveals earthquake displacements are critical to the 2018 3 Palu, Sulawesi Tsunami," 2019.

[69] P. L. F. Liu, I. Barranco, H. M. Fritz et al., "What we do and don't know about the 2018 Palu Tsunami—a future plan," in *Proceedings of the AGU Fall Meeting 2018*, Washington, DC, USA, December 2018.

[70] M. Carvajal, C. Araya-Cornejo, I. Sepúlveda, D. Melnick, and J. S. Haase, "Nearly instantaneous tsunamis following the M_w 7.5 2018 palu earthquake," *Geophysical Research Letters*, vol. 46, no. 10, p. 5117, 2019.

[71] US Geological Survey, *M_w 7.5 Palu earthquake, Indonesia*, US Geological Survey, Reston, VA, USA, 2018, https://earthquake.usgs.gov/earthquakes/eventpage/us1000h3p4/executive#executive.

[72] Geoscope Observatory, *M_w 7.5 Earthquake, Sulawesi 2018/09/28 10:02:43 UTC*, http://geoscope.ipgp.fr/index.php/en/catalog/earthquake-description?seis=us1000h3p4, 2018.

[73] A. Sas-Uhrynowski, H. Karatayev, S. Mroczek, and O. Karagodina, "Research of the secular variation of the geomagnetic field on Polish and Belarus territory," *Prace IGiK, Tom XLVII*, vol. 100, pp. 25–34, 2000.

[74] J. Marianiuk and J. Reda, *Results of Geomagnetic Observations*, Publications of the Institute of geophysics, Polish Academy of Science, C-79 (328), Belsk, Poland, 2001.

[75] A. Czyszek and J. Czyszek, *Results of Geomagnetic Observations, Hel, 2000*, Publications of the Institute of geophysics, Polish Academy of Science, Warszawa, Poland, 2002.

[76] H. Kahmen, *Elektronische Messverfahren in der Geodäsie. Grundlagen und Anwendungen*, Verlag Karsruhe, Gliwice, Poland, 1978.

[77] J. Skeivalas, E. K. Paršeliūnas, D. Šlikas et al., "Predictive models for identification of parameters of seismic vibrations by applying the theory of covariance functions," *Indian Journal of Physics*, vol. 95, 2019.

[78] J. Skeivalas, V. Turla, and M. Jurevicius, "Predictive models of the galaxies' movement speeds and accelerations of movement on applying the Doppler effect," *Indian Journal of Physics*, vol. 93, no. 1, pp. 1–6, 2019b.

[79] K. R. Koch, *Einführung in die Byes-Statistik*, Springer-Verlag Berlin Heidelberg, Berlin, Germany, 2000.

[80] J. Skeivalas and E. Parseliunas, "On identification of human eye retinas by the covariance analysis of their digital images," *Optical Engineering*, vol. 52, no. 7, Article ID 073106, 2013.